

Submitted to Nuclear Physics

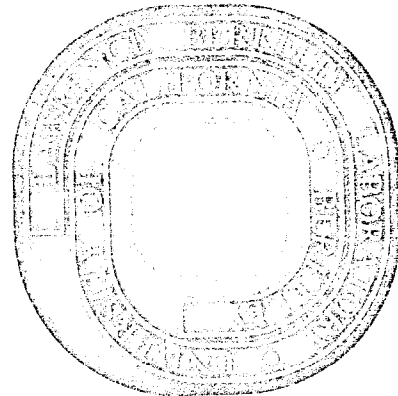
LBL-556  
(Slac-Pub-4043)  
Preprint

A MULTI-REGGE MODEL APPLIED TO  
HIGH-ENERGY INCLUSIVE PHOTOPRODUCTION

Clifford Risk, William P. Swanson, and  
Jerome H. Friedman

December 1974

AEC Contract No. W-7405-eng-48



A MULTI-REGGE MODEL APPLIED TO HIGH-ENERGY  
INCLUSIVE PHOTOPRODUCTION\*Clifford Risk<sup>†</sup>Lawrence Berkeley Laboratory and Department of Mathematics  
University of California, Berkeley, California 94720

William P. Swanson

Stanford Linear Accelerator Center, Stanford, University  
Stanford, California 94305Jerome H. Friedman<sup>††</sup>Lawrence Berkeley Laboratory, University of California  
Berkeley, California 94720

## ABSTRACT

We compare inclusive photoproduction data in the energy range  $E_{\gamma} = 9.0 - 18.0$  GeV to the multi-Regge model. The model incorporates vector-dominance coupling of the photon, the Chew-Pignotti algorithm for charge assignment, and correct treatment of n-body phase space. A technique of ordering the particles according to longitudinal momentum is used to enhance features of the data and provide a more sensitive test of the model. We compare the model to mass distributions, separation of particles in rapidity, longitudinal momentum distributions, topological cross-sections and charge orderings of secondaries. A reasonable description of the data is achieved, using parameters derived from pp and  $K^+p$  experiments.

---

\*Supported by the U. S. Atomic Energy Commission.

<sup>†</sup>Participating guest at LBL.

<sup>††</sup>Now at Stanford Linear Accelerator Center, Stanford, California 94305.

At high accelerator energies, where collision cross sections are dominated by high-multiplicity events, one cannot hope to comprehend interactions in terms of specific exclusive processes as has been widely and successfully attempted at lower energies. The suggestions of Feynman<sup>(1)</sup> and Yang<sup>(2)</sup> that these processes be studied through their inclusive characteristics then become appealing. By summing over many exclusive processes, one loses specific details about each individual process; but the compensating hope is that one may thus observe aggregate features<sup>(3)</sup> which arise from underlying dynamics, and which may not be apparent in specific channels.

This paper applies this approach to a high-energy photoproduction experiment performed using the SLAC 2-meter streamer chamber with hydrogen target.<sup>(4)</sup> An 18-GeV bremsstrahlung beam is used and at these energies a majority of events (about 5/6) have neutral particles. Thus the photon energy  $E_\gamma$  is unknown for most events. For each event we therefore calculate a surrogate "visible" photon energy  $E_{\text{vis}} \equiv |\Sigma \vec{P}_i|$ , where the index  $i$  refers to charged tracks. For the comparison described here we accept events having  $E_{\text{vis}} \geq 9.0$  GeV. The events retained for this study are produced by photons in the range  $E_\gamma = 9 - 18$  GeV (3075, 5205, 1151, and 160 of 3, 5, 7, and 9-prong events, respectively). The events are weighted to account for different film samples and individual geometrical configuration. We have arbitrarily normalized the data presented here such that 5-prong events have unit average weight.

The multi-Regge model we use is similar to that used earlier to compare to high-energy  $K^+p$  and  $pp$  experiments.<sup>(5)</sup> However, the coupling of the photon to the multi-Regge chain requires particular

tion. The "elastic" process  $\gamma p \rightarrow \rho^0 + p$  makes an important contribution to the cross section. It has been extensively studied and described in terms of the vector-dominance model represented by the diagram of Fig. 1a. <sup>(6)</sup> This suggests that the coupling of the  $\gamma$  to a multi-Regge chain might take the form of Fig. 1b. Here a  $\rho^0$  is diffractively excited, in accordance with the vector-dominance picture, and the exchanged Pomeron then ties onto the multi-Regge chain. This chain is characterized by an "effective meson"  $m$  which propagates to the target proton sequentially emitting produced pions, in the spirit of the multi-Regge model of Chew and Pignotti. <sup>(7)</sup>

Finally, we include a "background" term to the  $\rho^0$ , characterized by Fig. 1c. We do not expect this diagram to accurately describe all aspects of the coupling of the  $\gamma$  other than through the  $\rho^0$ , but, within the multi-Regge framework, to dualistically represent the many other types of processes that can occur at the "photon end" of this chain.

To keep the model as simple as possible, we have not included in the present comparison a diagram involving baryon exchange (Fig. 1d). We have found that the net effect of such diagrams is to increase the cross section for high-multiplicity events relative to those of lower multiplicity, and also to increase the contribution of backward charged secondaries. In the present analysis, these effects are relatively small.

The matrix-element squared for the diagram of Fig. 1c is given

$$|A|^2 = (g^2)^{N-2} \prod_{i=1}^{N-1} \left[ \frac{s_i + b}{b} \right]^{2\alpha(t_i)} \beta^2(t_i) = (g^2)^{N-2} \prod_{i=1}^{N-1} P_i(s_i, t_i) \quad (1)$$

ere  $s_i$ ,  $t_i$  are the invariant sub-energy and momentum transfer squared for the  $i$ -th link,  $\alpha(t)$  and  $\beta(t)$  are the trajectory and residue of the exchanged Reggeon,  $g^2$  is the coupling constant and  $b$  is a constant chosen to be equal to one so that the matrix-element approaches phase space at low subenergies. The matrix-element squared for Diagram 1 is given by

$$BW(M, \Gamma) \cdot \sin^2 \theta_H \cdot \left[ \frac{M(\rho)}{M(\pi\pi)} \right]^{n(t)} \cdot e^{At} \cdot (s+1)^{2\alpha_P(t)}, \quad (2)$$

ere  $BW$  is a mass-dependent Breit-Wigner factor,  $\theta_H$  is the  $\rho$ -decay helicity angle,  $n(t)$  pertains to the  $\rho$ -mass shift, and the last two factors are related to the exchanged Pomeron. Detailed formulae and values of parameters used can be found in the work of Moffeit<sup>(6)</sup>. The matrix-element squared for the diagram of Fig. 1b is obtained by replacing the first two propagators  $P_1$  and  $P_2$  of Eq. 1 by the appropriate form of Eq. (2).

The parameters of the trajectory  $\alpha(t)$ , residue  $\beta(t)$ , and  $m$ - $m$ - $\pi$  coupling constant  $g^2$  are all fixed in advance by previous multi-Regge analyses of  $K^+p$  and  $pp$  reactions.<sup>(5)</sup> (See Table 1) Hence we have only three free parameters: the overall normalizations of Diagrams 1(a, b, c). All other features of the model predictions are then fixed. To evaluate our predictions, we sum incoherently over the diagrams of Fig. 1, performing the  $n$ -body phase space integrals with the LBL program MCGE.<sup>(8)</sup> Monte Carlo events in the energy range  $E_\nu = 9.0 - 18.0$  GeV are generated in this manner. An event weight is calculated, based on the matrix element corresponding to a diagram of Fig. 1, multiplied by the bremsstrahlung shape. For each such simulated event, charges are assigned by the Chew-Pignotti charge algorithm.<sup>(7)</sup>

An important advantage of this procedure is that we incorporate in the model the identical instrumental and programmed selections that the data contain. Specifically, the simulated events are treated as if neutral secondaries are unobserved and a selection on  $E_{vis}$  is imposed, as it is for the real events. The simulated events are generated with correct masses; in the comparison with data all charged particles are later assigned the mass of the charged pion,  $\mu$ , both in real and simulated events.

In an attempt to more sensitively examine the characteristics of secondaries presumed to emerge from various portions of the multi-Regge chain, we have ordered the charged secondaries according to  $P_L$ . Thus, we define: 1  $\equiv$  particle with smallest  $P_L$  (lab), 2  $\equiv$  particle with next smallest  $P_L$ , etc. Figure 2 (a-f) shows the invariant mass distributions of neighboring tracks which have been ordered in this fashion. Separate plots are shown for neighbors with equal and unequal charges. For three-prong events, invariant-mass distributions for the pair of "slowest" particles (1 and 2) are shown in Fig. 2a and for the two fastest particles (2 and 3) in Fig. 2b. Most striking is the peak near the  $\rho^0$  mass in the  $M(2, 3)$  distribution for unlike charges. As found elsewhere, the mass is shifted towards a value lower than the accepted  $\rho^0$  mass. This is conveniently achieved in the model through the mass-dependent factor suggested by Ross and Stodolsky, included in Eq. (2).<sup>(9)</sup>

Note that the average values of the masses in Fig. 2a are large a reflection of the small  $M(2, 3)$  mass and the presumed Pomeron line of Fig. 1a and 1b. The model underestimates the mass distribution for unlike charges in  $M(2, 3)$  at high mass and in  $M(1, 2)$  at low mass

These events could come from specific quasi-two processes that are not reproduced by our multi-Regge background.

In Fig. 2 (c-f), the corresponding mass plots for five-prong events are made. Here, the noticeable experimental feature is the peak in the  $M(4, 5)$  mass distribution near the  $\rho^0$  mass. The theory overestimates the distribution for unlike charges and underestimates that for like charges. These discrepancies could be reduced by allowing charged mesons to be produced at the  $\gamma$ -end of Fig. 1c, a possibility arising naturally within the framework of the ABFST version of the multiperipheral model<sup>(12)</sup> (see Fig. 1e). The net effect is to increase the probability that the first two charged tracks emerging have charges of the same sign. This detailed end-effect is perhaps the major inadequacy of the Chew-Pignotti model in our comparison.

In Fig. 2e, a small peak appears in the  $M(3, 4)$  data at the  $\rho^0$  mass. To within the statistics of the Monte Carlo, this peak does not appear to arise from the "end"  $\rho^0$  of Fig. 1b emerging slowly, but is instead produced "internally". Its source could be a coupling of the form  $\gamma \rightarrow A_{1,2}$  (plus pions)  $\rightarrow \rho^0$  (plus pions) or  $\gamma \rightarrow \rho^0 \rightarrow \rho^0 \pi^+ \pi^-$ .<sup>(10)</sup>

For each event, both in experiment and theory, we also plot the separation in rapidity between neighboring tracks (Fig. 2g). (We define rapidity as  $w \equiv (P_L - E) / \sqrt{P_T^2 + \mu^2}$ .) The distributions seen may be regarded as a reflection of the mass distributions of Fig. 2 (a-f). The noticeable features for three-prong events are the large separation between 2 and 3 when they are of opposite charge. For five-prong events, the low subenergies result in small separations in rapidity. A common feature of Fig. (2g) is that like-charged neighbors are always further separated than unlike-charged neighbors.

In Fig. 3 we show the longitudinal momentum distribution for positive and negative tracks for 3, 5, and 7 prong events, (Figs. a, b, c) as well as summed over all events (Fig. 3d). We note that distributions of positive and negative tracks are very similar in high-momentum range. This is a consequence of the photon fragmenting into positive and negative secondaries with substantially the same probability. On the other hand, we note an essential difference between the two distributions near  $P_L = 0.0$ , in that the positive tracks have a large peak. This effect is due to the high elasticity of the proton, which leads to the proton emerging at  $P_L$  near zero in the laboratory. (We remark that even at large  $P_L$  the positive distribution tends to remain somewhat larger than that for the negative secondaries.)

As the multiplicity increases, (see Fig. 3b, 3c), the range of  $P_L$  contracts as the energy is shared among an increasing number of particles. Moreover, the difference to be seen between the positive and negative distributions becomes smaller as the effect of the proton-charge is reduced by the presence of additional charged secondaries.

The model description of the data both in magnitude and shape is quite good. In the multi-Regge model, the  $t$ -cut off in the propagators leads to a Poisson-type of multiplicity dependence, with the constant  $g^2$  fixing the average. From Ref. 5, we have  $g^2 = 7$  in advance, and see from Fig. 3 that relative magnitudes of the various multiplicities is adequately described.<sup>(12)</sup> In addition, the shapes of the  $P_L$  distributions are accounted for except at  $P_L \lesssim 0$ . In the 3-prong distribution (Fig. 3a), the model underestimates the slow  $\pi^-$  distribu-



gs. 2a, b. In the 7-prong distribution (Fig. 3c), the low prediction at  $P_L \sim 0$  could be improved by including baryon exchange.

In Table 2, we present the relative topological cross sections. The three-prong cross section is underestimated, a reflection of the presence of background in Fig. 2b. The 7-prong cross section is somewhat underestimated also, although this could be improved with the inclusion of baryon exchange; the effect of baryon exchange would be to raise the higher-multiplicity cross sections through the inclusion of low- $Q$  resonances.

As still a further way of investigating the correlations among the charged secondaries, we have evaluated the probability for various configurations of the charged particles in the three-prong events.

These data and the theoretical predictions are given in Table 3. Here

it is seen that the configuration having the negative track as number 1 (west) is greatly depressed, compared to the other possible configurations. This of course reflects the  $\gamma$ -coupling to a neutral system and the proton's elasticity. The theory tends to exaggerate this effect, which is a reflection of our underestimation of the high-mass background in Fig. 2a and our underestimation of the  $P_L$  distribution of negative secondaries at small  $P_L$  (Fig. 3a).

The contributions of Diagrams of Fig. 1 to the total cross section (omitting strange-particle production) required are about 12  $\mu\text{b}$ , 10  $\mu\text{b}$  and 45  $\mu\text{b}$ , respectively. These amounts refer to the sample before the  $E_{\text{vis}}$  selection is made. Thus it would seem that Diagrams 1a and 1c are of roughly comparable magnitude and that  $\gamma$ -( $\rho \rightarrow 2\pi$ ) coupling does not dominate higher multiplicity processes to the degree that it dominates the three-prong events.

A significant result of this study is that, using parameters  $\alpha(t)$ ,

provision for photon coupling, multibody photoproduction is reasonably described by the multi-Regge model. Thus the model suggests a connection between these different experiments through their common parameters. This observation provides evidence that the underlying dynamics in  $\gamma p$ ,  $K^+ p$  and  $pp$  multibody production may be fundamentally similar, except for the particular manner in which the beam particle couples onto the production mechanism.

The novel approach we have taken to compare this type of data with theory (namely, the ordering of tracks by longitudinal momenta and the event-by-event generation and handling of Monte-Carlo event exactly like the data) is a method that may be of great use in the analysis of similar experiments.

In conclusion, we emphasize that the generally adequate description of the data by this model arises from the model incorporating several characteristics of photoproduction—(1) elasticity of incident particles (as reflected in the  $P_L$  distributions of Fig. 3), (2)  $t$  cut-off (as reflected in the prong cross sections), (3)  $\gamma$ - $\rho^0$  coupling (as seen in Fig. 2 and Fig. 3), (4) correct evaluation of  $n$ -body phase space (a prerequisite for any detailed comparison of a model to data), (5) and the bremsstrahlung spectrum and neutral pion production (which are features of this experiment). Quite likely, these characteristics can be built into other types of models, such as the thermodynamic and diffractive models.<sup>(1,3)</sup> While the present comparison does offer a theoretical framework for the nature of the underlying production mechanism, tests must be formulated that can distinguish between the features unique to multiperipheralism and those unique to the other models. Work on this will be reported elsewhere.

### ACKNOWLEDGMENTS

We are indebted to R. F. Mozley and members of the SLAC Streamer-Chamber Group, M. Davier, I. Derado, D. C. Fries, F. F. Liu, A. C. Odian, J. Park, F. Villa, and D. E. Yount, for the use of the photoproduction data. We have had helpful discussions with K. C. Moffeit of SLAC. One of us (C.R.) is grateful to R. F. Mozley and SLAC for financial support through which part of the present research was performed.

REFERENCES

R. P. Feynman, in Proceedings of the Third International Conference--High Energy Collisions, Stony Brook, 1969, edited by C. N. Yang et al., (Gordon and Breach, New York, 1969); Phys. Rev. Letters 23, 1415 (1969).

J. Benecke, T. T. Chou and C. N. Yang, Phys. Rev. Letters 25, 1072 (1970).

Well-known examples of such aggregate features are the limited transverse momenta, and high-energy behavior of total cross sections.

Related material based on these data may be found in: W. P. Swanson, M. Davier, I. Derado, D. C. Fries, F. F. Liu, R. F. Mozley, A. C. Odian, J. Park, F. Villa, and D. E. Yount, Phys. Rev. Letters 27, 1472 (1971); W. P. Swanson, W. Ko, R. L. Lander, C. Risk, R. R. Ross and D. B. Smith, Comparison of the Inclusive  $\pi^-$  Distributions from  $\gamma p$ ,  $K^+ p$  and  $pp$  Collisions, SLAC-PUB-979 (October, 1971), submitted to Phys. Rev. Letters. The experimental arrangement is similar to that described in M. Davier, I. Derado, D. Drickey, D. Fries, R. Mozley, A. Odian, F. Villa and D. Yount, Phys. Rev. D1, 690 (1970).

- a). J. H. Friedman and C. Risk, UCRL-20278 (1971), submitted to Physical Review;
- b). C. Risk and J. H. Friedman, Phys. Rev. Letters 27, 353 (1971). See for example (a) Cambridge Bubble Chamber Group, Phys. Rev. 146, 994 (1966); (b) Aachen-Berlin-Bonn-Hamburg-Heidelberg-München Collaboration, Phys. Rev. 175, 1669 (1968);

(c) SLAC-Berkeley-Tufts Collaboration, J. Ballam, H. H. Bingham, G. B. Chadwick, W. B. Fretter, R. Gearhart, Z. G. T. Guiragossian, M. Menke, R. H. Milburn, K. C. Moffeit, J. J. Murray, W. J. Podolsky, M. S. Rabin, A. H. Rosenfeld, P. Seyboth, A. Shapira, C. K. Sinclair, I. O. Skillicorn, R. Windmolders and G. Wolf, Phys. Rev. Letters 24, 955 (1970); K. C. Moffeit, Ph.D. Thesis, UCRL-19 890 (1970), unpublished. (d) J. Park, M. Davier, I. Derado, D. C. Fries, F. F. Liu, R. F. Mozley, A. C. Odian, W. P. Swanson, F. Villa and D. Yount, SLAC-PUB-972 (1971), submitted to Nuclear Physics.

G. F. Chew and A. Pignotti, Phys. Rev. 176, 2112 (1968).

J. H. Friedman, Group A Programming Note P-189, Lawrence Berkeley Laboratory (1969), unpublished.

M. Ross and L. Stodolsky, Phys. Rev. 149, 1172 (1966). We use the t-dependent formulation derived from the analysis of K. C. Moffeit (Ref. 6c). This mass-shift is usually interpreted physically as due to an interference effect between  $\rho$ -production amplitudes; P. Söding, Phys. Letters 19, 702 (1965); A. S. Krass, Phys. Rev. 159, 1946 (1967).

Evidence for other photon couplings, possibly of this type, is presented in M. Davier, I. Derado, D. C. Fries, F. F. Liu, R. F. Mozley, A. C. Odian, J. Park, W. P. Swanson, F. Villa, and D. Yount, "The Reaction  $\gamma p \rightarrow \pi^+ \pi^- \pi^+ \pi^- p$  at High Energy

and Photon Dissociation into 4 Pions", submitted to the International Symposium on Electron and Photon Interactions at High Energies, Cornell University, Ithaca, New York, August 23-27, 1971. Indirect evidence may be found in a study of  $\bar{p}p$  annihilations at rest ( $\bar{p}p \rightarrow \rho^0 \pi^+ \pi^-$ ) J. Díaz, Ph. Gavillet, G. Labrosse, L. Montanet, W. P. Swanson, P. Villemoes, M. Bloch, P. Frenkiel, C. Ghesquiere, E. Lillestøl and A. Volte, Nuclear Physics B16, 329 (1970).

11. L. Bertocchi, S. Fubini, and M. Tonin, Nuovo Cimento 25, 626 (1962); D. Amati, A. Stanghellini, and S. Fubini, *ibid* 26, 896 (1962).
12. In the present comparison, we have the magnitude of Fig. 1a  $t$  adjust in reproducing the three prong cross-section.
13. For single particle distributions, the  $t$ -cut off of multiperipheralism is equivalent to a  $P_T$  cut-off in these models.

Table 1. Parameters in the model

	Meson		Baryon	
$\beta(t)$	$e^{2.1t}$	$t > -0.3$	$e^{1.5t}$	$t > 0.2$
	$c e^{0.3t}$	$t < -0.3$	$c' e^{0.2t}$	$t < 0.2$
$\alpha(t)$	$t + 0.5$	$t > -0.6$	$t + \alpha_0$	$t > 0$
	$0.5t + 0.3$	$-2 < t < -0.6$	$0.5t + \alpha_0$	$-0.5 < t < 0$
	$0.25t - 0.2$	$t < -2.$	$0.2t + \alpha_0 - 0.15$	$t < 0.5$
			$\alpha_0 = -1$	if $s > 6$
			$\alpha_0 = -2$	if $s < 6$

The value of  $\alpha_0$  gives an adequate fit to a parametrization of the backward  $\pi^-p$  elastic cross section,  $d\sigma/du \sim (s/s_0)^{2\alpha_0-2}$  for  $s < 8 \text{ GeV}^2$ . It is not the intercept of the canonical  $\Delta^{++}$  trajectory, which governs  $d\sigma/du$  for  $s \geq 8 \text{ GeV}^2$ . The constants  $c, c'$  simply ensure continuity. In Eq. (1), we used  $g^2 = 7$ .

Table 2. Relative topological cross sections for  $E_{vis} > 9$  GeV.

Topology	Experiment	Theory
3-prong	7570	6008
5-prong	5205	5482
7-prong	2803	2254

Table 3. Relative charge ordering of 3-prong events ( $E_{vis} > 9$  GeV).

Track ordering 1 2 3	Experiment	Theory
- + +	10%	3%
+ - +	48%	47%
+ + -	42%	50%

F  
R  
di  
F  
ti  
ir  
C  
a  
tr  
a  
s  
ii  
ii  
e  
F  
e  
ti  
ti

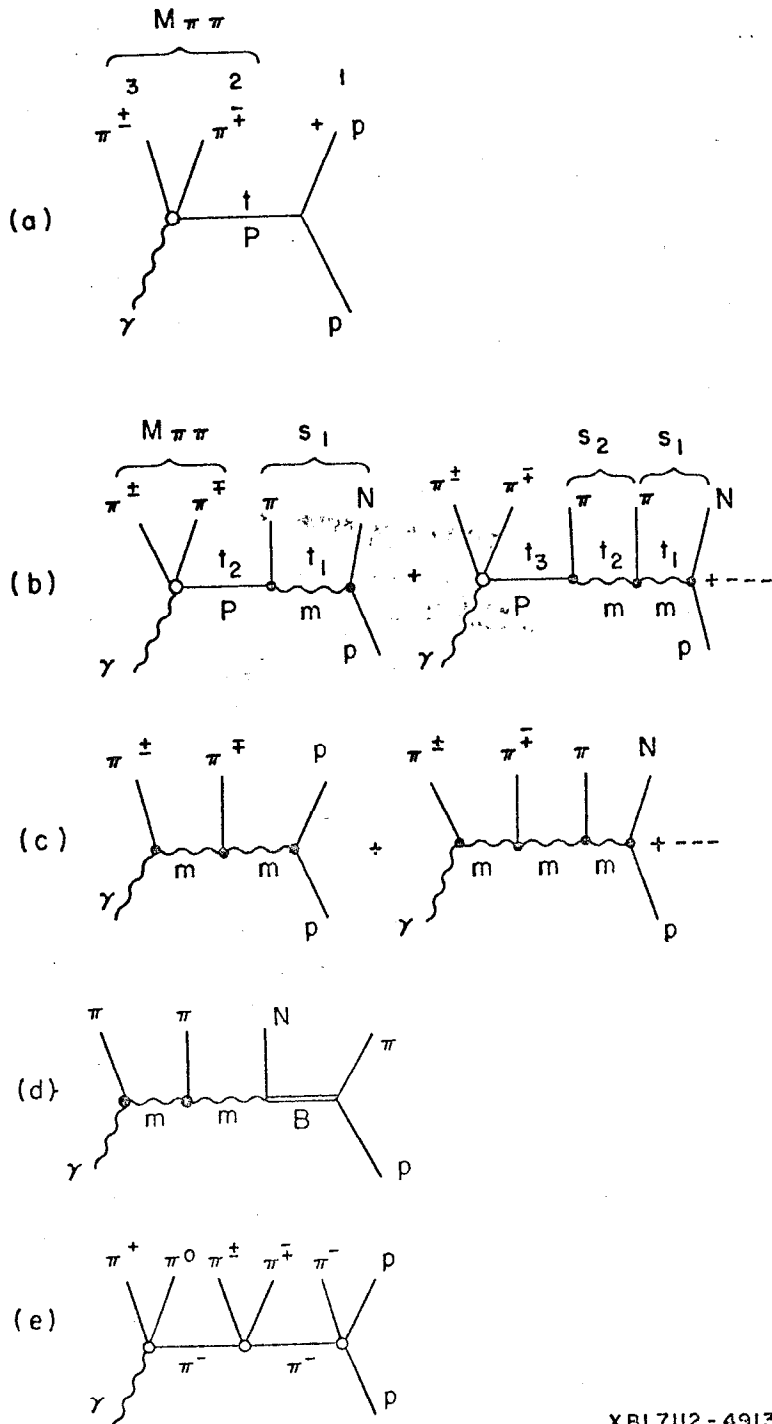


## FIGURE CAPTIONS

1. Multi-peripheral diagrams for photoproduction; (a)-(c) Multi-  
e diagrams used in this report; (d) baryon exchange; (e) A BFST  
am.

2. (a)-(f) Invariant-mass distributions of two-particle combina-  
. All particles are assumed to be pions and are ordered accord-  
o laboratory longitudinal momentum (1 = smallest  $P_L$ , etc.).  
binations of adjacent tracks are shown. Possible neutral particles  
gnored. In each panel (a)-(f) the upper distribution contains neu-  
dipions, and the lower (shaded) doubly charged ( $++$  or  $--$ ). Curves  
he multi-Regge model described in the text. Panels (a) and (b)  
3-prong events; (c) - (f) show 5-prongs. (g) Average spacing  
pidity  $\Delta w_{i,i+1}$  of adjacent charged particles. See text for def-  
on of rapidity used. The error bar in Fig. (e) shows a typical  
r in the Monte Carlo calculation. Normalization discussed in text.

3. Longitudinal momentum distributions in 3-, 5-, a 7-prong  
ts and in all events for positive tracks (solid lines) and negative  
ks (dashed lines). Histograms—experimental data; curves—  
retical predictions. Normalization discussed in text.



XBL7112-4913

Fig. 1

$E_{vis} > 9$  GeV. 6903 events

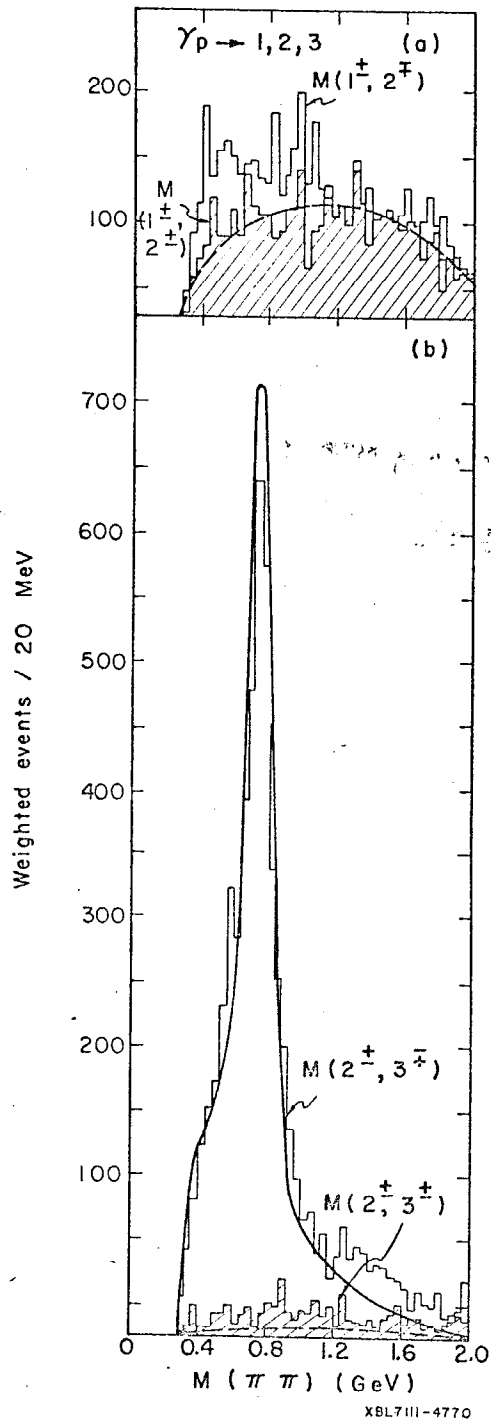


Fig. 2 a-b

$E_{vis} > 9 \text{ GeV}$  5205 events

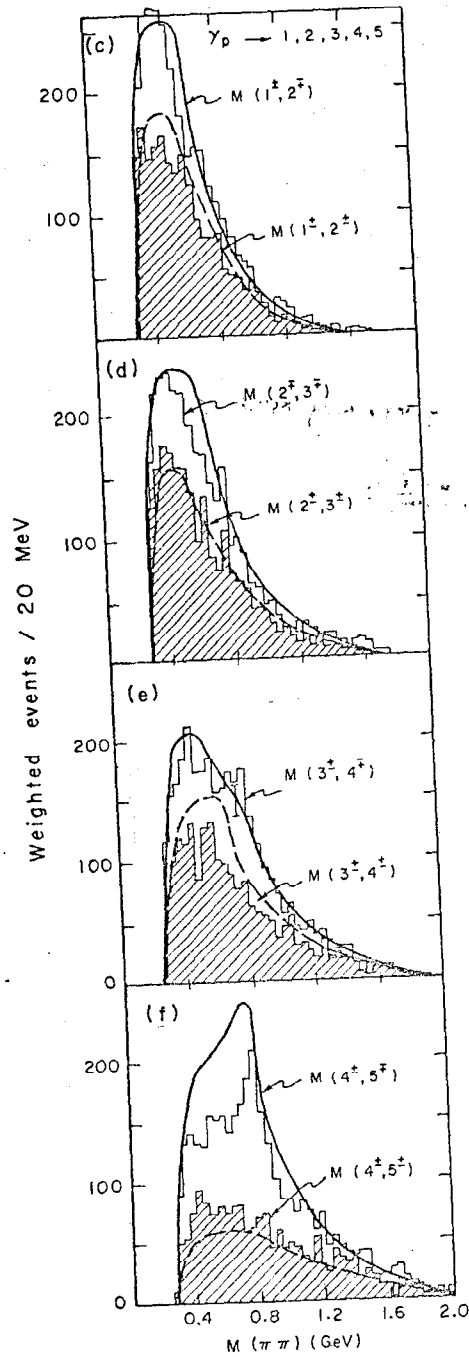
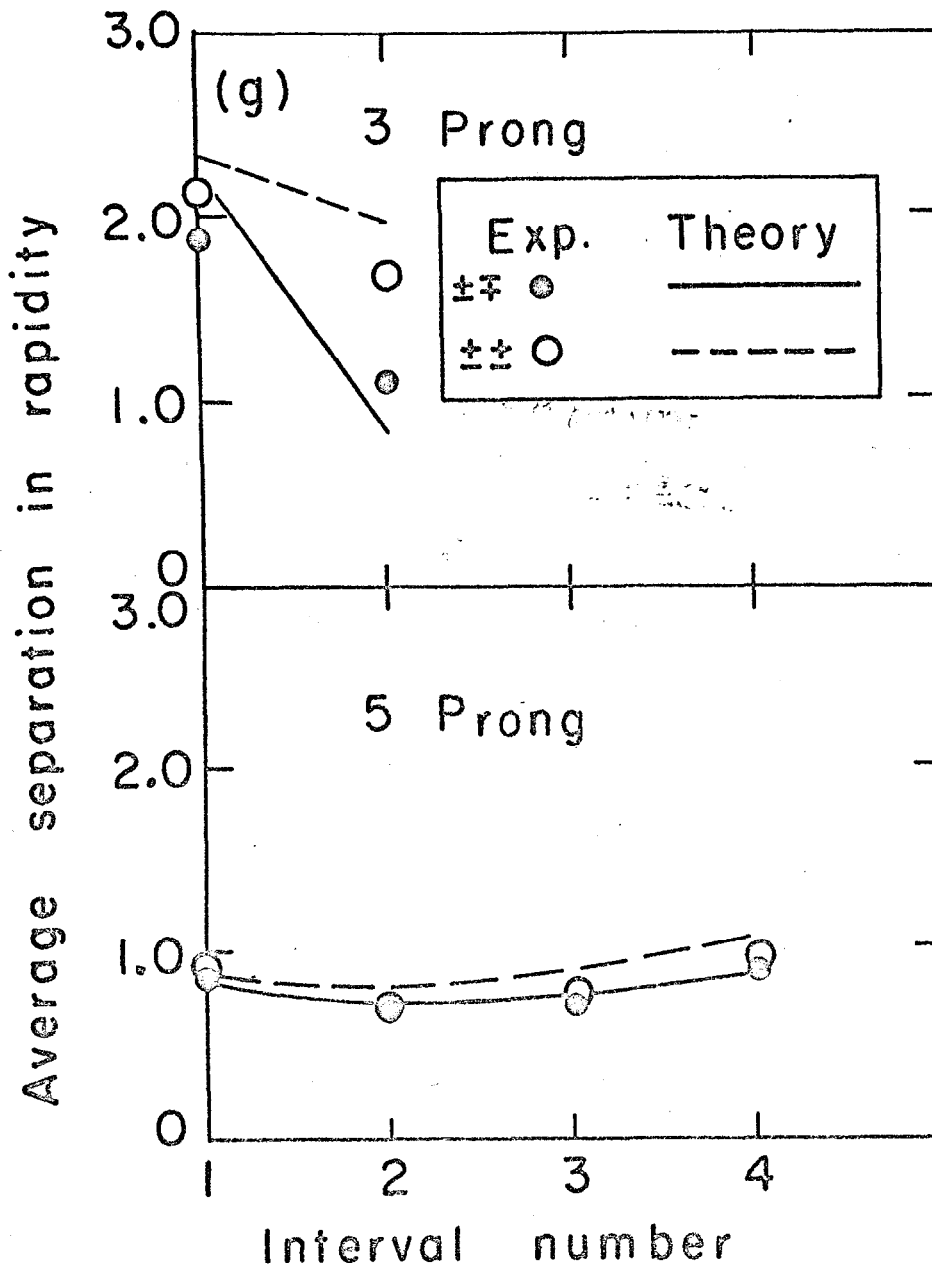
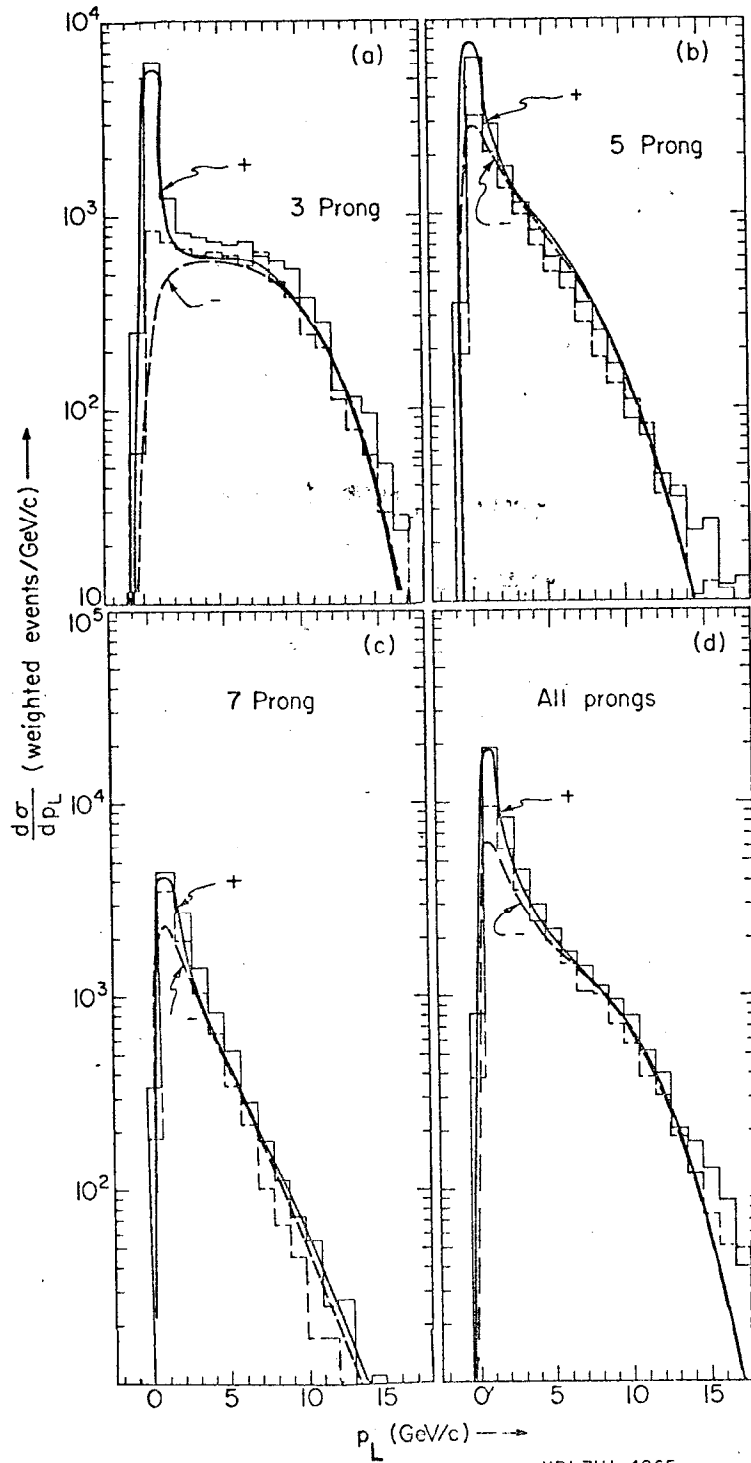


Fig. 2 c - f



XBL 7112-4914

Fig. 2 g



XBL7111-4865

Fig. 3

LEGAL NOTICE

*This report was prepared as an account of work sponsored by the United States Government. Neither the United States nor the United States Atomic Energy Commission, nor any of their employees, nor any of their contractors, subcontractors, or their employees, makes any warranty, express or implied, or assumes any legal liability or responsibility for the accuracy, completeness or usefulness of any information, apparatus, product or process disclosed, or represents that its use would not infringe privately owned rights.*